ASTEROIDS

The Lucy flyby of (52246) Donaldjohanson: A bilobed asteroid with tumbling rotation

Simone Marchi[1]*, Harold F. Levison[1], Keith S. Noll[2,3], John R. Spencer[1], Thomas S. Statler[4], Olivier S. Barnouin[5], James F. Bell III[6], Edward B. Bierhaus[7], Richard Binzel[8], William F. Bottke[1], Daniel Britt[9], Michael E. Brown[10], Marc W. Buie[1], Philip R. Christensen[6], Neil Dello Russo[5], Joshua P. Emery[11], William M. Grundy[11,12], Victoria E. Hamilton[1], Carly Howett[3,13], Hannah H. Kaplan[2], Katherine Kretke[1], Tod R. Lauer[14], Brian H. May[15], Stefano Mottola[16], Catherine B. Olkin[17], Martin Pätzold[18], Joel Wm. Parker[1], Frank Preusker[16], Silvia Protopapa[1], Dennis C. Reuter[2], Stuart J. Robbins[1], Julien Salmon[1], Amy A. Simon[2], S. Alan Stern[19], Jessica M. Sunshine[20], David Vokrouhlický[21], Harold A. Weaver[5], Harrison Agrusa[22,23], Emily S. Costello[24], Masatoshi Hirabayashi[25], Fiona Nichols-Fleming[26], Jennifer E. C. Scully[27], Anne Verbiscer[28], Coralie Adam[29], John Andrews[1], Kevin E. Berry[2], Emma Birath[1], Rich Burns[2], Russell Carpenter[2], Mark Effertz[7], Kristen Francis[7], Jeroen Geeraert[29], Sheila Gray[7], Katie Hegedus[7], David Kaufmann[1], Brian A. Keeney[1], Thomas Kennedy[7], Jim McAdams[29], Matthew Montanaro[30], Jon Pineau[31], Devin Poland[2], Eric Sahr[29], Ishita Solanki[1], Dale Stanbridge[29], Brian Sutter[7], Michael Vincent[1]

The main belt asteroid (52246) Donaldjohanson (DJ) is a likely member of the Erigone asteroid family. This implies that DJ is a fragment of a larger parent body that was destroyed in a collision about 155 million years ago. We report observations taken during a flyby of DJ by the Lucy spacecraft. We found that DJ is composed of two heavily cratered lobes, connected by a smoother neck, with overall dimensions 8.8 kilometers (km) by 4.4 km by 3.1 km. The crater density is consistent with the Erigone family's age, except for craters <0.4 km, which have been preferentially erased. DJ rotates slowly in a tumbling state, likely owing to spin-down by radiative forces. Surface spectra show iron-bearing phyllosilicates, indicating moderate aqueous evolution on the parent body.

The Lucy spacecraft (*1*) flew past the inner main belt asteroid (52246) Donaldjohanson (hereafter DJ) on 20 April 2025. This flyby included a sequence of observations (*2*) using the spacecraft's closed-loop terminal tracking system, which autonomously points the instruments at the target during the flyby (*3*). Lucy's closest approach to DJ was 961.4 km at 17:51:16 UT, when the relative speed was 13.4 km s^{-1}. DJ was only observed on the inbound leg of the flyby; observations were terminated 31 s before closest approach to avoid pointing the instruments at the Sun.

DJ's orbit indicates that it probably belongs to the Erigone asteroid family, which formed 115 million to 225 million years ago (Ma), most likely around ≈155 Ma, from the break-up of a larger parent asteroid (*4*–*6*). The orbits of the Erigone family members have a mean semimajor axis of ≈2.37 astronomical units (au), placing them in the inner main belt, close to a region where asteroids are scattered onto near-Earth orbits (*7*). Spectroscopic observations indicate that Erigone family members have a similar composition to some Mighei-type carbonaceous chondrite (CM) meteorites. About half of the observed family members have spectra exhibiting an absorption band at 0.7 μm, which is interpreted as being due to silicates that have been altered by the presence of liquid water (*8*).

Light curve and rotation state

In the 59 days before the encounter, we obtained unresolved images of DJ using Lucy's Long Range Reconnaissance Imager (L'LORRI) instrument (*9*). The light curve (reflected flux as a function of time) from these images (Fig. 1) has a main periodicity of 252.6 ± 0.4 hours and an amplitude of about 1 magnitude, consistent with previous ground-based observations (*10*). We identified an additional second period at 455.2 ± 0.9 hours (*11*). We interpret this as evidence that DJ is in non–principal axis (NPA) rotation, an excited state in which the instantaneous rotation axis is not aligned with a principal inertia axis, so the body undergoes free precession and nutation. The predicted timescale for DJ to achieve a principal axis rotation state is about 20 billion years (Gyr) (*11*), much longer than the ≈155 Myr age of the family, so in the absence of additional processes, we expect the excited NPA rotation state to persist once initiated.

We constructed a dynamical rotation model (*11*) to reproduce the observed light curve, which indicates that DJ undergoes prograde rotation around an axis inclined ≈5° from the perpendicular of the orbital plane (obliquity angle). DJ's orbit is outside the mean semimajor axis of the Erigone family, consistent with migration driven by the anisotropic emission of thermal photons [Yarkovsky effect (*6*)]. DJ's slow spin and low obliquity are both compatible with the expected effects of thermal torques from reflection and remission of sunlight [Yarkovsky-O'Keefe-Radzievskii-Paddack (YORP) effect (*12*, *13*)].

NPA rotation has been observed in other slow-rotating small bodies, including the near-Earth asteroid (4179) Toutatis, which has a similar size [4.75 km by 1.95 km; (*14*)], shape, and long rotation period [≈176 hours (*15*, *16*)]. Proposed origins of Toutatis's perturbed rotational state include close approaches to terrestrial planets, radiative effects, or collisions (*17*–*19*). DJ's orbit does not come close to any planets, so only the latter two mechanisms are applicable.

We found no sign of cometary activity in the inbound images. No satellites or moons were found; we excluded any bodies with a diameter >7.2 m within 200 km from DJ and with a diameter >15 m throughout DJ's ≈700-km diameter Hill sphere (*11*).

Surface morphology and shape

L'LORRI images taken during the flyby (*11*) show that DJ has a bilobed shape and a surface exhibiting complex geological features (Fig. 2). The highest-resolution imaging (5.2 m $pixel^{-1}$) shows three distinct terrains: two cratered terrains comprising most of the imaged small and large lobes and a smoother terrain covering part of the neck

[1]Solar System Science and Exploration Division, Southwest Research Institute, Boulder, CO, USA. [2]NASA Goddard Space Flight Center, Greenbelt, MD, USA. [3]Planetary Science Institute, Tucson, AZ, USA. [4]NASA Headquarters, Washington, DC, USA. [5]Johns Hopkins University Applied Physics Laboratory, Laurel, MD, USA. [6]School of Earth and Space Exploration, Arizona State University, Tempe, AZ, USA. [7]Lockheed Martin Space, Littleton, CO, USA. [8]Department of Aeronautics and Astronautics, Massachusetts Institute of Technology, Cambridge, MA, USA. [9]Department of Physics, University of Central Florida, Orlando, FL, USA. [10]Division of Geological and Planetary Sciences, California Institute of Technology, Pasadena, CA, USA. [11]Lowell Observatory, Flagstaff, AZ, USA. [12]Department of Astronomy and Planetary Science, Northern Arizona University, Flagstaff, AZ, USA. [13]Atmospheric, Oceanic and Planetary Physics, University of Oxford, Oxford, UK. [14]National Optical-Infrared Astronomy Research Laboratory, National Science Foundation, Tucson, AZ, USA. [15]London Stereoscopic Company, London, UK. [16]Institute of Space Research, German Aerospace Center, Berlin, Germany. [17]Fifth West Consulting, Niwot, CO, USA. [18]Freies Institut für Planetenforschung Köln, Cologne, Germany. [19]Space Sector, Southwest Research Institute, Boulder, CO, USA. [20]Department of Astronomy, Department of Geological, Environmental and Planetary Sciences, University of Maryland, College Park, MD, USA. [21]Astronomical Institute, Charles University, Prague, Czech Republic. [22]Université Côte d'Azur, Observatoire de la Côte d'Azur, French National Center for Scientific Research, Laboratoire Lagrange, Nice, France. [23]Centre national d'études spatiales, Paris, France. [24]Hawaii Institute of Geophysics and Planetology, University of Hawaii at Manoa, Honolulu, HI, USA. [25]Daniel Guggenheim School of Aerospace Engineering, Georgia Institute of Technology, Atlanta, GA, USA. [26]Center for Earth and Planetary Studies, Smithsonian National Air and Space Museum, Washington, DC, USA. [27]Jet Propulsion Laboratory, California Institute of Technology, Pasadena, CA, USA. [28]Department of Astronomy, University of Virginia, Charlottesville, VA, USA. [29]Flight Dynamics Interplanetary Department, KinetX, Littleton, CO, USA. [30]Center for Imaging Science, Rochester Institute of Technology, Rochester, NY, USA. [31]Stellar Solutions, Denver, CO, USA. ***Corresponding author. Email: simone.marchi@swri.org**

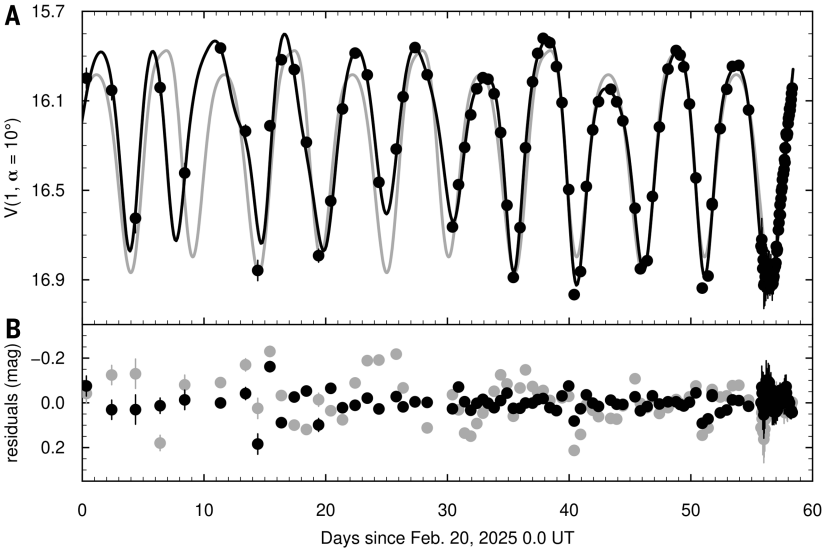

Fig. 1. Light curve of DJ. (**A**) V-band magnitudes (black circles) extracted from the L'LORRI imaging using a circular aperture. Error bars show 1σ uncertainties. Fluxes were converted to magnitudes that would be observed at 1 au from the spacecraft and from the Sun and then converted to the average solar phase angle (α) of 10° (*11*) (table S1). The gray line is a fifth-order Fourier model of the data using a single best-fitting period of 253.2 ± 0.5 hours. The black line is a third-order Fourier model with two periods, with best-fitting values of 252.6 ± 0.4 and 455.2 ± 0.9 hours. The two models have reduced-χ^2 values of 47.4 and 11.3, respectively. (**B**) Residuals between the data and the models in (A). Gray and black points are for the single-period and two-period models, respectively. The single-period residuals show systematic oscillations owing to the additional underlying period.

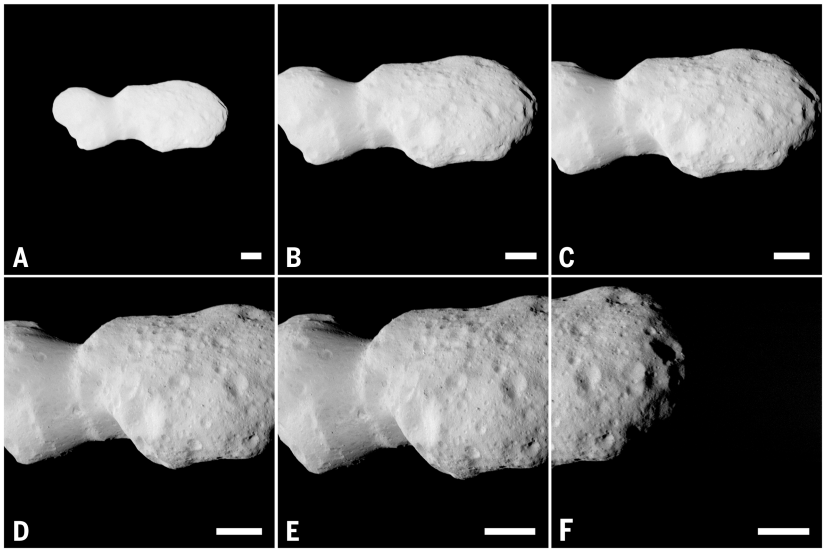

Fig. 2. L'LORRI images of DJ taken during the approach. (**A** to **F**) Six example visible images selected from the 268 (with ≥10-pixel mean diameter) acquired during spacecraft approach. The relative brightness changes as a result of the varying phase angle and exposure time (table S2). Scale bars are 1 km.

between the two lobes (Fig. 3A). We constructed a three-dimensional shape model using stereophotogrammetry applied to the image sequence (*11*) and used it to identify distinct regions on the surface (Fig. 3C). We define the neck terrain (NT) and small-lobe terrain (SLT) with a boundary that follows changes in local roughness and shadowing, indicating a change in local slopes (Fig. 3D). The large-lobe terrain (LLT) is also separated from the NT by a change in local slopes and topography. The NT region contains a ridge, which reaches the LLT-NT boundary near the northern limb (edge of the observed sunlit hemisphere).

We mapped craters on the observed surface in the closest approach images (*11*). The SLT and LLT have indistinguishable crater size-frequency distributions (SFDs; Fig. 4A), after accounting for observational biases (*11*); we focus our discussion on the LLT because of its higher number of identified craters. The crater SFD of the LLT (Fig. 4A) has a slope discontinuity at crater diameter $D = 0.2$ to 0.4 km. Craters larger than $D =$ 0.4 km follow a power law with a slope of approximately −2 (Fig. 4A), consistent with crater equilibrium (crater density nearly constant with time), a behavior also observed on asteroid (253) Mathilde (*20*). Craters with $D = 0.08$ to 0.4 km have a shallower power law slope of −1.4, indicating a lower density than expected for equilibrium. In this size range, the theoretical cumulative slope of crater populations that have not reached equilibrium is ≈−2.5, which has been observed on a young surface of asteroid (4) Vesta (*21*). A crater SFD slope of ≈−2.5 is also predicted by theoretical calculations based on the expected impactor SFD (later in this section). At $D = 0.08$ to 0.2 km, the crater distribution for DJ is shallower than those for craters of similar size on the near-Earth asteroid Bennu (Fig. 4A), which also have a higher spatial density.

The discontinuities and the shallow power law slopes for small craters could be due to measurement biases, an incorrect impactor SFD used for our calculations, or preferential erasure of small craters. Although lighting conditions and viewing angle can affect the identification of small craters (*22*), the similar slopes of the LLT and SLT SFDs (Fig. 4A) over terrains with different viewing geometry indicate that this effect is small for our observations (*11*). Craters on other asteroids are consistent with a single impactor SFD in the main belt (*23*, *24*), as assumed in our calculations. We therefore conclude that craters with $D \lesssim 0.4$ km have been preferentially erased.

We used the crater populations to constrain the target's cratering strength Y. We assumed that DJ's surface is no older than the parent Erigone asteroid family [115 to 225 Ma; (*6*)] and adopted expected impact rate and strength scaling laws (*11*, *23*, *25*). Using the observed spatial density of craters with $D > 0.4$ km, we calculated (*11*) $Y \leq 4 \times 10^4$ Pa (Fig. 4B), with the nominal family age 155 Ma corresponding to $Y \leq 10^4$ Pa. This value is only an upper limit for a surface in cratering equilibrium, because an unknown number of craters have been erased by subsequent impacts.

For $Y = 10^4$ Pa, the age of the LLT derived from small craters (0.08 to 0.2 km) is 20 to 40 Ma, depending on the crater size range used (Fig. 4B) (*11*). This implies that craters <0.2 km in diameter are erased on timescales <40 Ma, well after the formation of the Erigone family. The small rubble-pile asteroids Bennu and Ryugu have cratering strengths <100 Pa (*26*, *27*). If DJ had such a low strength, craters would form under self-gravity, and the corresponding age of the LLT would be ≈1 Ma, which we regard as too short for potential erasing mechanisms to operate (*11*). We therefore conclude that DJ's surface strength is probably substantially higher than those of Bennu and Ryugu (*28*, *29*), which have broadly similar surface compositions. DJ is ~10 times larger (in diameter) than Bennu and Ryugu, so it might not share their shattered rubble-pile interior structure (*29*, *30*). Individual submeter-sized boulders on Ryugu have strengths up to 10^5 Pa (*31*).

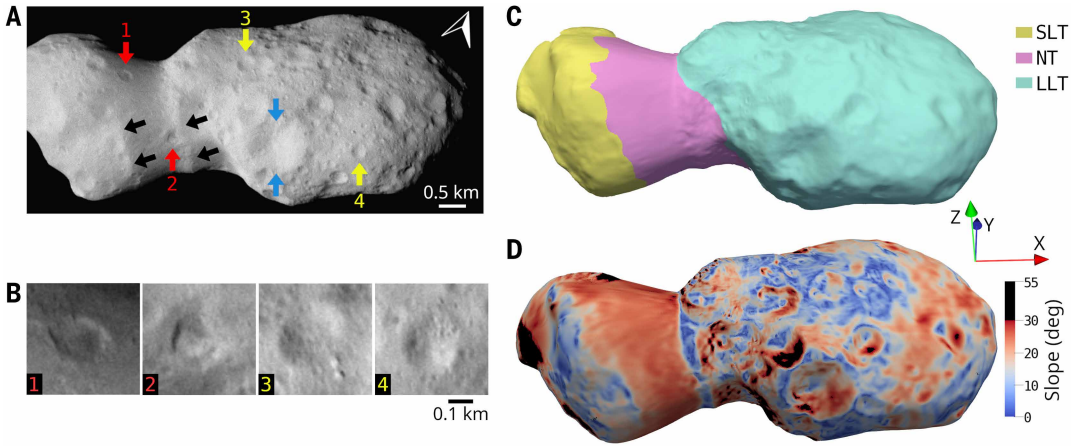

Fig. 3. DJ's shape, geological units, and surface slopes. (**A**) L'LORRI visible image taken at a range of 1762.6 km and a phase angle of 18.4°. The compass arrow indicates the North Celestial Pole. Black arrows indicate a slope change and a ridge (left and right arrows, respectively). Red arrows indicate heavily modified craters on the neck, and yellow arrows indicate unmodified craters of similar size on the large lobe. Blue arrows indicate a ≈1-km crater. (**B**) Zoomed-in views of four example craters labeled in (A), all on the same scale: 1 is a flat-floored crater, 2 is a crater partially filled by material from the nearby ridge, and 3 and 4 are craters with unmodified morphology. (**C**) Shape model of the imaged portion of DJ. Colors indicate the three terrains that we defined in the text: SLT (yellow), NT (pink), and LLT (cyan). (**D**) Shape model with colors indicating the slope angles, computed for a uniform density of 1200 kg m^{-3} [as for Bennu and Ryugu; (*35*)] and a spin period of 252 hours (around the *z* axis; green orientation arrow). The color map is capped at 30°, with higher slopes indicated in black (maximum slope is 55°).

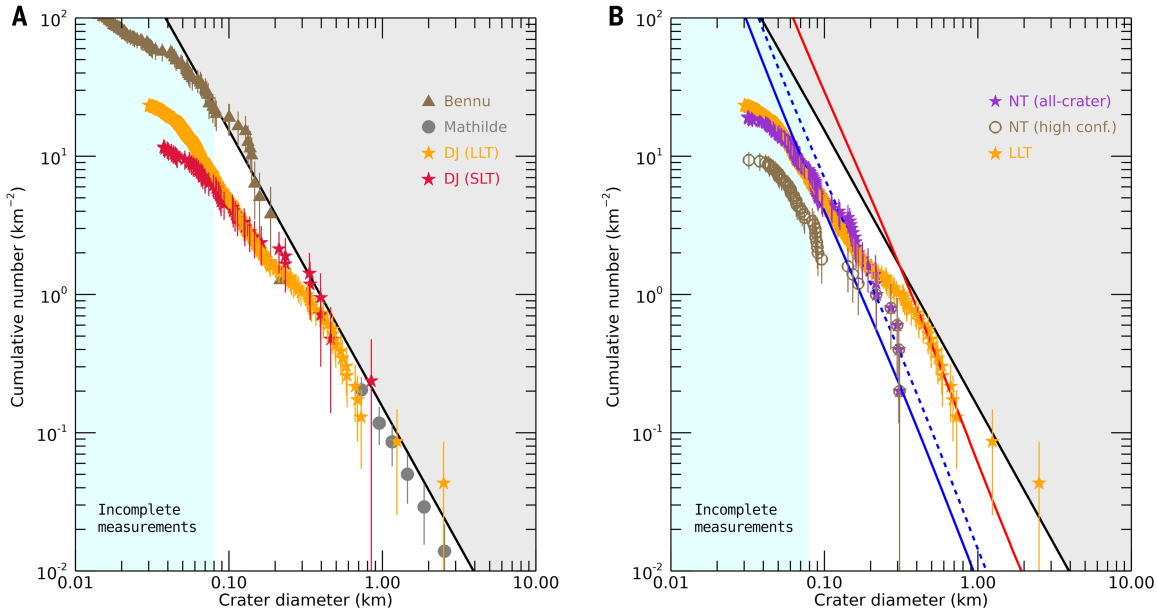

Fig. 4. Crater size-frequency distributions on DJ. (**A**) SFDs of craters identified on the large and small lobes (orange and red stars, respectively). The black line indicates an empirical equilibrium level [10% of geometric saturation; (*23*)], and the gray-shaded region is in equilibrium. The cyan-shaded region indicates the size range where our crater identification is incomplete. Brown triangles and gray circles are craters on Bennu (*30*) and Mathilde (*20*) for comparison, respectively. Error bars are 1σ. (**B**) Same as (A) but overlain with the SFDs for craters in the NT. Violet stars are all craters, and brown open circles are high-confidence craters only. Lines are the best-fitting production functions for LLT $D > 0.4$ km (solid red), LLT $D = 0.08$ to 0.1 km (solid blue), and LLT $D = 0.15$ to 0.20 km (dashed blue), assuming $Y = 10^4$ Pa.

The NT region is much smoother than the SLT and LLT (Fig. 3A). There are craters in the NT, but they have a more degraded morphology than craters in the LLT and SLT (Fig. 3B). We mapped NT craters and assigned a confidence level (high or low) to each. The resulting SFD for the NT (Fig. 4B) has a wavy structure, which we ascribe to ambiguity in crater identification and low-number statistics. The NT all-crater population is consistent with that of both the LLT and SLT for $D = 0.08$ to 0.2 km, so we suggest that the crater erasure occurred globally. If small craters within the LLT and SLT were erased <40 Ma, DJ's surface was modified more recently than its formation age. The modified morphology of some of the NT craters implies that mass wasting has occurred in the NT more recently than the global erasing event. By fitting a model to the high-confidence craters on the NT, we estimate that the more recent local crater degradation occurred <20 Ma. This localized mass wasting and crater degradation might have been triggered by a larger impact (*11*, *32*–*34*) (Fig. 3A).

We constructed a three-dimensional shape model of DJ by applying stereophotogrammetry to the visible (front) side. To approximate the

unobserved (rear) side, we modeled the asteroid as two contacting ellipsoids, with dimensions fitted to the front hemisphere. The front and rear parts were fused, and the resulting shape was manually refined to match the observed body contours [limb and terminator (*11*)]. This model has a volume of ~58 km^3 and overall dimensions 8.8 km by 4.4 km by 3.1 km. Assuming a density of 1200 kg m^{-3} [as for Bennu and Ryugu; (*35*)], DJ's mass is about 7×10^{13} kg.

Combining this shape model with the spin period (252 hours) and assuming uniform density, we calculated that local slopes are dominated by self-gravity (Fig. 3D), with minimal contributions from centrifugal force. The NT has a largely uniform slope, averaging 25°. This uniform and high slope [typical internal friction slopes are <35°; (*36*)] indicates that the neck region has probably experienced one or more episodes of movement of material from the small lobe toward the large lobe (figs. S1 and S2). The side of the ridge facing the small lobe has a low slope (<10°), as we expect for material relocated to that location by gravity (fig. S1A). DJ likely had a higher spin rate in the past (*11*); we calculated that the low slope in this region could be maintained unless centrifugal force exceeds gravity, at spin periods of ~4 to 5 hours, in which case the flow of loose material would be directed from the large to the small lobe (fig. S1B). There is a well-defined change in slope between the SLT and NT (Fig. 3D), so we do not see any morphological evidence for any past reversal of direction in the local acceleration.

Surface composition

The Linear Etalon Imaging Spectral Array (LEISA) instrument (*37*) acquired near-infrared imaging spectra during the flyby. We constructed global average spectra using low–phase angle (≈3°) data taken during the approach phase to minimize the effect of illumination changes. Thermal emission was removed during data reduction (*11*). Figure 5 compares the LEISA spectrum to archival ground-based observations using the Infrared Telescope Facility and the Lowell Discovery Telescope (*11*). The LEISA spectrum exhibits an absorption feature centered at 2.790 ± 0.009 μm with a depth of 24.2 ± 0.5%. We identify this as the 2.8-μm band of OH in hydrated minerals. The ground-based spectrum has an additional absorption band at 0.7 μm, which is also indicative of hydrated minerals.

DJ's spectrum is similar to other carbonaceous (C-type) asteroids in the Erigone family (Fig. 5A), which probably formed from the same parent body (*6*). DJ's 2.8-μm band is consistent (in position and shape) with those of a subset of CM meteorites that have experienced moderate aqueous alteration. Figure 5, B and C, compares DJ's spectrum to those of the CM meteorite QUE 97990 and an Ivuna-type carbonaceous chondrite (CI) meteorite (*38*). DJ's band position is more consistent with the CM comparison spectrum. The combination of 0.7- and 2.8-μm features is characteristic of surface mineralogy dominated by iron-rich phyllosilicate minerals (*38*, *39*).

Fe-bearing phyllosilicates are commonly produced by incomplete aqueous alteration. Further alteration reactions cause Fe cations to be progressively replaced by Mg (*40*), weakening the 0.7-μm band and shifting the 2.8-μm band to shorter wavelengths. The spectra of Bennu and Ryugu show no 0.7-μm band and have phyllosilicate bands centered near 2.7 μm (*29*, *41*–*43*), consistent with Mg-rich phyllosilicates, indicating a greater degree of aqueous alteration on their parent bodies than for DJ. This implies that alteration reactions on DJ's parent body were halted in the early stages, perhaps because of insufficient water or heat to continue.

These results indicate differences in the internal evolution of the parent bodies of C-type asteroid families within the inner main belt. Possible explanations include formation in different regions of the Solar System or at different times before being captured onto their current orbits (*44*, *45*).

Implications for the origin of DJ

Our results indicate that DJ has a complex history. The presence of Fe-bearing phyllosilicates provides support for DJ being a member of the Erigone asteroid family. DJ's spectrum is similar to those of CM meteorites, although the Erigone family is not expected to be a major

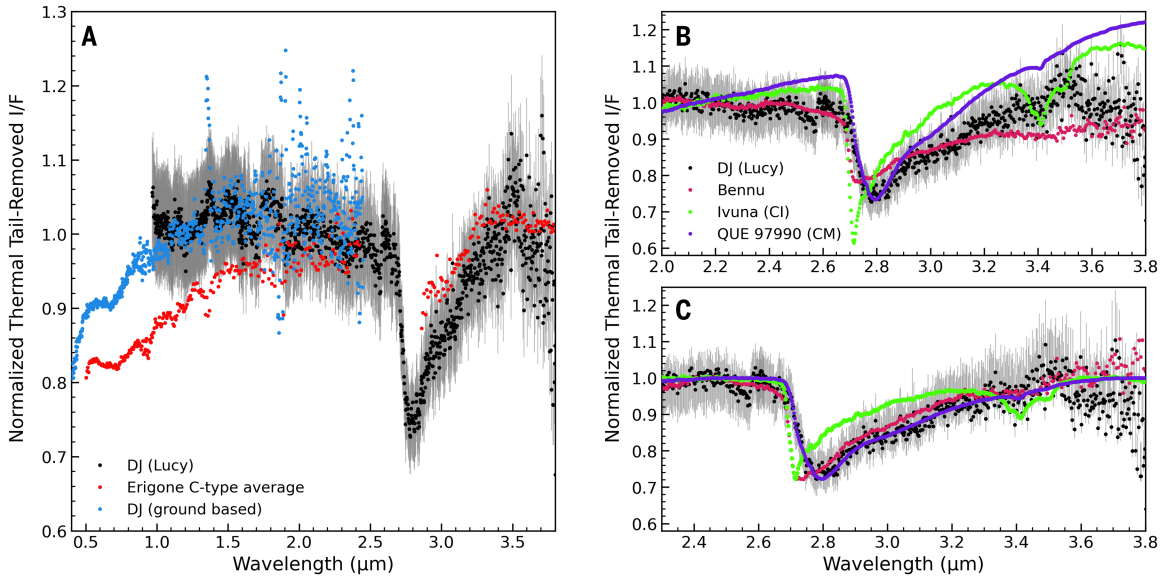

Fig. 5. Spectra of DJ and comparison asteroids. The normalized thermal tail–removed radiance factor (I/F) is the reflected component of the spectrum after subtraction of the long-wavelength thermal emission, normalized in the wavelength range 2.12 to 2.15 μm. (**A**) Black dots are the global average spectrum of DJ observed with LEISA. Gray error bars show 1σ uncertainties, which are assumed to be 7%. Blue dots are the average ground-based spectrum of DJ. All spectra have been smoothed with a Gaussian filter (*11*). Red dots are the average spectra of C-type asteroids in the Erigone family [constructed from 54 visible spectra (*8*), 13 near-infrared spectra (*46*), and one 3-μm spectrum of Erigone itself (*47*)]. (**B**) Zoomed-in view of the unsmoothed 2.8-μm phyllosilicate band for DJ (black dots), compared with CI (Ivuna; green dots) and CM (QUE 97990; violet dots) meteorites (*38*) and the asteroid Bennu [red dots; (*41*)]. (**C**) Continuum-divided spectra shown in the 2.3- to 3.8-μm region. The comparison spectra are scaled to match the band depth of DJ in the 2.8-μm region.

source of meteorites (*6*). DJ's slow spin, NPA rotation, and low obliquity can be explained by Yarkovsky and YORP effects (*11*).

We propose the following scenario for the formation and evolution of DJ. The parent body of the Erigone family was ≈80 km in diameter and was destroyed by a ≈20-km impactor at ≈155 Ma (*6*). DJ's bilobed shape probably arose from the accretion of fragments from this breakup event. This left DJ with an initial spin period of ≪10 hours.

The YORP effect then slowed DJ's rotation and shifted its spin axis toward low obliquity. After 20 to 60 Myr, DJ's spin period reached ≈10 hours, causing slopes in the neck region to fail. The resulting widespread mass movement toward both lobes produced the ridge and smoothed the neck region.

Sometime later (<40 Ma), craters smaller than 0.4 km were globally erased, possibly owing to seismic shaking by an impact. Localized mass wasting on the neck continued, degrading the morphology of many craters without altering the small crater SFD. From 80 to 120 Myr after formation, DJ's rotation entered its current NPA state, with a spin period of 100 to 200 hours (*11*).

Similar evolutionary processes have been documented for other near-Earth asteroids, including Bennu, Ryugu, and Toutatis. Because DJ is a member of a young asteroid family, we were able to constrain the timescales of these processes.

REFERENCES AND NOTES

1. H. F. Levison *et al.*, *Planet. Sci. J.* **2**, 171 (2021).
2. C. B. Olkin *et al.*, *Planet. Sci. J.* **2**, 172 (2021).
3. H. F. Levison *et al.*, *Nature* **629**, 1015–1020 (2024).
4. D. Vokrouhlický, M. Brož, W. F. Bottke, D. Nesvorný, A. Morbidelli, *Icarus* **182**, 118–142 (2006).
5. F. Spoto, A. Milani, Z. Knežević, *Icarus* **257**, 275–289 (2015).
6. S. Marchi *et al.*, *Planet. Sci. J.* **6**, 59 (2025).
7. W. F. Bottke *et al.*, *Icarus* **247**, 191–217 (2015).
8. D. Morate *et al.*, *Astron. Astrophys.* **586**, A129 (2016).
9. H. A. Weaver *et al.*, *Space Sci. Rev.* **219**, 82 (2023).
10. M. Ferrais, thesis, Aix Marseille Université (2022).
11. Materials and methods are available as supplementary materials.
12. W. F. Bottke Jr., D. Vokrouhlický, D. P. Rubincam, D. Nesvorný, *Annu. Rev. Earth Planet. Sci.* **34**, 157–191 (2006).
13. D. Vokrouhlický, W. F. Bottke, S. R. Chesley, D. J. Scheeres, T. S. Statler, in *Asteroids IV*, P. Michel, F. E. DeMeo, W. F. Bottke, Eds. (Univ. Arizona Press, 2015), pp. 509–531.
14. J. Huang *et al.*, *Sci. Rep.* **3**, 3411 (2013).
15. J. Spencer, *Icarus* **117**, 71–89 (1995).
16. R. S. Hudson, S. J. Ostro, *Science* **270**, 84–86 (1995).
17. D. J. Scheeres, F. Marzari, A. Rossi, *Icarus* **170**, 312–323 (2004).
18. D. Vokrouhlický, S. Breiter, D. Nesvorný, W. F. Bottke, *Icarus* **191**, 636–650 (2007).
19. T. Henych, P. Pravec, *Mon. Not. R. Astron. Soc.* **432**, 1623–1631 (2013).
20. C. R. Chapman, W. J. Merline, P. Thomas, *Icarus* **140**, 28–33 (1999).
21. S. Marchi *et al.*, *Planet. Space Sci.* **103**, 96–103 (2014).
22. S. J. Robbins, M. R. Kirchoff, L. R. Ostrach, *Geophys. Res. Lett.* **52**, e2024GL110570 (2025).
23. S. Marchi, C. R. Chapman, O. S. Barnouin, J. E. Richardson, J.-B. Vincent, in *Asteroids IV*, P. Michel, F. E. DeMeo, W. F. Bottke, Eds. (Univ. Arizona Press, 2015), pp. 725–744.
24. W. F. Bottke *et al.*, *Astron. J.* **160**, 14 (2020).
25. K. A. Holsapple, K. R. Housen, *Icarus* **187**, 345–356 (2007).
26. M. Arakawa *et al.*, *Science* **368**, 67–71 (2020).
27. M. E. Perry *et al.*, *Nat. Geosci.* **15**, 447–452 (2022).
28. Y. Zhang *et al.*, *Nat. Commun.* **13**, 4589 (2022).
29. S. Sugita *et al.*, *Science* **364**, 252 (2019).
30. E. B. Bierhaus *et al.*, *Nat. Geosci.* **15**, 440–446 (2022).
31. M. Grott *et al.*, *Nat. Astron.* **3**, 971–976 (2019).
32. R. Greenberg, M. C. Nolan, W. F. Bottke Jr., R. A. Kolvoord, J. Veverka, *Icarus* **107**, 84–97 (1994).
33. J. Richardsonjr, H. Melosh, R. Greenberg, D. Obrien, *Icarus* **179**, 325–349 (2005).
34. D. Obrien, R. Greenberg, J. Richardson, *Icarus* **183**, 79–92 (2006).
35. J. H. Roberts *et al.*, *Planet. Space Sci.* **204**, 105268 (2021).
36. Y. Zhang *et al.*, *Astrophys. J.* **857**, 15 (2018).
37. D. C. Reuter *et al.*, *Space Sci. Rev.* **219**, 69 (2023).
38. D. Takir *et al.*, *Meteorit. Planet. Sci.* **48**, 1618–1637 (2013).
39. F. Vilas, M. J. Gaffey, *Science* **246**, 790–792 (1989).
40. K. Tomeoka, H. Y. McSween Jr., P. R. Buseck, *Antarct. Meteor. Res.* **2**, 221 (1989).
41. V. E. Hamilton *et al.*, *Nat. Astron.* **3**, 332–340 (2019).
42. A. A. Simon *et al.*, *Science* **370**, eabc3522 (2020).
43. K. Kitazato *et al.*, *Science* **364**, 272–275 (2019).
44. A. Morbidelli, K. J. Walsh, D. P. O'Brien, D. A. Minton, W. F. Bottke, in *Asteroids IV*, P. Michel, F. E. DeMeo, W. F. Bottke, Eds. (Univ. Arizona Press, 2015), pp. 493–507.
45. T. Hopp *et al.*, *Sci. Adv.* **8**, eadd8141 (2022).
46. B. Harvison *et al.*, *Icarus* **412**, 115973 (2024).
47. A. S. Rivkin, C. A. Thomas, E. S. Howell, J. P. Emery, *Astron. J.* **150**, 198 (2015).
48. H. A. Weaver *et al.*, Lucy LOng Range Reconnaissance Imager (L'LORRI) Donaldjohanson Raw Data. *NASA Planetary Data System* (2025); https://doi.org/10.26007/DBSX-3W41.
49. D. Reuter *et al.*, Lucy Ralph Linear Etalon Imaging Spectral Array (L'Ralph LEISA) Donaldjohanson Raw Data. *NASA Planetary Data System* (2025); https://doi.org/10.26007/szzg-aw56.

ACKNOWLEDGMENTS

We thank the entire Lucy mission team for their hard work and dedication. We thank paleoanthropologist D. Johanson, who found the Lucy hominin fossil, for his enthusiasm and engagement in the flyby of the asteroid bearing his name. We thank D. Minton and two other anonymous reviewers for their valuable comments. **Funding:** The Lucy mission is financed through the NASA Discovery program on contract no. NNM16AA08C; M.P. was supported by the Deutsche Raumfahrtagentur DLR-RFA, Bonn, under grant 50OW2401; D.V. was supported by the Czech Science Foundation (grant 25-16507S); E.S.C. acknowledges support from NASA grant 80NSSC25K7725; M.H. acknowledges support from NASA grant 80NSSC25K0011; F.N.-F. acknowledges support from NASA grant 80NSSC25K7723; J.E.C.S. acknowledges support from NASA grant 24-LUCYL4PSP-0031, and their work was carried out at the Jet Propulsion Laboratory, California Institute of Technology, under a contract with NASA (80NM0018D0004); A.V. acknowledges support from NASA grant 80NSSC25K0159; H.A. acknowledges support of the Lucy Participating Scientist program and financial support from the Centre national d'études spatiales, France (ROR: https://ror.org/04h1h0y33); and M.P. acknowledges support from the Bundesministerium für Forschung, Technologie und Raumfahrt, Berlin, via the German Space Agency RFA, Bonn, under grant 50OW2401. **Author contributions:** S.Ma., H.F.L., K.S.N., and J.R.S. wrote the manuscript. O.S.B., J.F.B.III, E.B.B., W.F.B., D.B., N.D.R., S.J.R., H.A., E.S.C., M.H., F.N.-F., J.E.C.S., H.A.W., and D.V. contributed to imaging acquisition, geological and cratering analyses supported by K.K. and M.P.; R.Bi., P.R.C., J.P.E., W.M.G., V.E.H., C.H., H.H.K.,C.B.O., S.P., D.C.R., A.A.S., J.M.S., and M.M. contributed to the acquisition and interpretation of spectra data; M.E.B. led the satellite search; S.A.S. led the activity search; T.S.S., T.R.L., B.H.M., S.Mo., F.P., A.V., and M.W.B. contributed to shape modeling, rotation state and photometry; C.A., K.E.B., M.E., K.F., J.G., S.G., K.H., T.K., J.M., E.S., D.S., and B.S. contributed to spacecraft navigation and operation; and J.W.P., E.B., D.K., B.A.K., I.S., J.P., M.V., and J.S. contributed to observational sequence planning and data downlink data processing and archiving. J.A., R.Bu., R.C., and D.P. are project managers for the Lucy mission. All authors read and discussed the manuscript. **Competing interests:** C.B.O. was a paid consultant to the Southwest Research Institute. All other authors declare that they have no competing interests. **Data, code, and materials availability:** Lucy mission data are available at the NASA Planetary Data System archive at https://pds-smallbodies.astro.umd.edu/data_sb/missions/lucy/. We used the L'LORRI data (*48*) and LEISA data (*49*); the IDs of the specific images and spectra are provided in tables S1 and S2. Our derived shape model of DJ is available at https://naif.jpl.nasa.gov/pub/naif/pds/pds4/lucy/lucy_spice/spice_kernels/dsk/. No physical materials were generated in this work.

SUPPLEMENTARY MATERIALS

science.org/doi/10.1126/science.aec0503
Materials and Methods; Figs. S1 to S5; Table S1 and S2; References (*50*–*74*)

Submitted 4 September 2025; accepted 23 April 2026

10.1126/science.aec0503

The Lucy flyby of (52246) Donaldjohanson: A bilobed asteroid with tumbling rotation

Simone Marchi, Harold F. Levison, Keith S. Noll, John R. Spencer, Thomas S. Statler, Olivier S. Barnouin, James F. Bell, III, Edward B. Bierhaus, Richard Binzel, William F. Bottke, Daniel Britt, Michael E. Brown, Marc W. Buie, Philip R. Christensen, Neil Dello Russo, Joshua P. Emery, William M. Grundy, Victoria E. Hamilton, Carly Howett, Hannah H. Kaplan, Katherine Kretke, Tod R. Lauer, Brian H. May, Stefano Mottola, Catherine B. Olkin, Martin Pätzold, Joel Wm. Parker, Frank Preusker, Silvia Protopapa, Dennis C. Reuter, Stuart J. Robbins, Julien Salmon, Amy A. Simon, S. Alan Stern, Jessica M. Sunshine, David Vokrouhlický, Harold A. Weaver, Harrison Agrusa, Emily S. Costello, Masatoshi Hirabayashi, Fiona Nichols-Fleming, Jennifer E. C. Scully, Anne Verbiscer, Coralie Adam, John Andrews, Kevin E. Berry, Emma Birath, Rich Burns, Russell Carpenter, Mark Effertz, Kristen Francis, Jeroen Geeraert, Sheila Gray, Katie Hegedus, David Kaufmann, Brian A. Keeney, Thomas Kennedy, Jim McAdams, Matthew Montanaro, Jon Pineau, Devin Poland, Eric Sahr, Ishita Solanki, Dale Stanbridge, Brian Sutter, and Michael Vincent

Science **392** (6804), . DOI: 10.1126/science.aec0503

Editor's summary

The Erigone asteroid family was probably produced by a catastrophic collision that broke up a parent body. Marchi *et al*. present results from the Lucy spacecraft flyby of the small asteroid Donaldjohanson, a likely member of the Erigone family, finding that it has a bilobed shape and a smooth neck region. Small craters have been preferentially erased, possibly by seismic shaking after a larger impact. The asteroid is slowly tumbling, not simply rotating, which the authors model as being due to a resonance that arose while it gradually slowed from an initially fast spin rate. — Keith T. Smith